Adv. Polar Upper Atmos. Res., 15, 117-127, 2001

Propagation modes and source locations of the auroral kilometric radiation (AKR) identified by using the wave distribution function method

Akira Hosotani[1], Takayuki Ono[1], Atsushi Kumamoto[1] and Hiroshi Oya[2]

[1] *Department of Geophysics, Graduate School of Science, Tohoku University, Aoba, Aramaki, Aoba-ku, Sendai 980-8578*
[2] *Fukui University of Technology, Gakuen 3-6-1, Fukui 910-8505*

Abstract: The propagation characteristics of Auroral Kilometric Radiation (AKR), the propagation mode, power flux as well as propagation direction, have been analyzed by applying the wave distribution function method to the Poynting Flux measurement data obtained by the PWS system onboard the Akebono (EXOS-D) satellite. The results revealed that the power flux of O-mode waves was about 10 percent of the X-mode wave intensity in strong AKR emissions. The X-mode AKR waves tend to fill inside the radiation cone of an auroral field line. On the other hand, O-mode AKR showed two different propagation directions, one was directed to almost 90° with respect to the local magnetic field and the other showed angle in the vicinity of 40°. It was shown that the source locations of O-mode AKR waves with the propagation angle of about 40° located close to the source of the intense X-mode AKR waves.

1. Introduction

Auroral Kilometric Radiation (AKR) is the most prominent natural radio emission from the earth. AKR was identified as a radiation associated with the development of auroral phenomena by Gurnett (1974), since then, extensive studies on the source location as well as the generation mechanism of AKR have been carried out.

The early satellite observations claimed that AKR is simply a X-mode radio wave (Gurnett and Green, 1978; Kaiser *et al.*, 1978). Oya and Morioka (1983), however, showed that AKR has O-mode propagation based on the observation from the Jikiken satellite. Hashimoto (1984) explained this confliction by a difference of refraction indices of X-mode and O-mode waves in the plasma cavity based on the ray tracing analysis of X-mode and O-mode waves. Mellott *et al.* (1984) showed the coexistence of both X-mode and O-mode waves, however, X-mode wave intensities are generally stronger by a factor of 50 based on the DE-1 satellite observations. They also found that the propagation of X-mode AKR is directed to an angle less than about 50° to the geomagnetic field line, while O-mode AKR is typically observed with larger propagation angles.

Proposals for the generation mechanism of AKR can be categorized into two basic processes. One is a mechanism generating directly in the form of electromagnetic

waves based on the Cyclotron Maser Instability (CMI) proposed by Wu and Lee (1979). Another mechanism is a linear conversion process from electrostatic waves generated by a beam plasma instability to electromagnetic waves that was originately proposed by Oya (1971, 1974), and applied to the generation mechanism of AKR by Benson (1975). However, the mode conversion mechanism has not been interpreted as a major process because the linear conversion mechanism leads a different result for the power ratio of O-mode to X-mode waves, since observations showed that the dominant propagation mode of AKR is X-mode. However, a recent theoretical study has solved this difficulty by applying the Doppler Mode Conversion (DMC) process improved by Oya (1990), who took into account the Doppler shift due to the velocity shear between plasma media. Thus, it becomes difficult to clarify these proposed mechanisms only from the viewpoint of the polarization of AKR because both theories predict the coexistence of X-mode and O-mode waves. Therefore, it is necessary to clarify these mechanisms by examining the detailed propagation characteristics of AKR emissions.

The propagation characteristics of AKR were initiated by examining cut-off frequencies of AKR on spectrograms. More accurate observations were carried out based on the direction finding by analyzing polarization characteristics of AKR waves (Shawhan and Gurnett, 1982) and spin modulation effects of electric field antennas of the DE-1 satellite (Calvert, 1985). However, these methods still needed several assumptions for the identification. The Plasma Waves and Sounder experiment (PWS) onboard the Akebono satellite has the function of the measurement of the poynting flux of plasma waves (Morioka *et al.*, 1990). The waveform data obtained with the Poynting Flux measurement mode (PY mode) have been analyzed by using the Means method (Means, 1972) to identify the propagation characteristics of AKR. The Means method has a less ambiguity than previous observation techniques, however this method becomes inadequate in the case of multi-sources or the coexistence of X-mode and O-mode waves because the Means method requires a simple assumption of a monochromatic plane wave for the analysis of observed waveform data.

For the purpose to estimate the full propagation characteristics of AKR, in this paper, we applied the Wave Distribution Function (WDF) method introduced by Storey and Lefeuvre (1979, 1980) to the analysis of waveform data obtained with PY mode operation of the PWS system onboard the Akebono satellite. By applying the WDF method we analyzed the propagation mode, power and propagation direction of AKR waves. The results of the analysis have been applied to the identification of the source location of AKR waves.

2. Instrumentation

The Akebono satellite was launched into an eccentric polar orbit with initial apogee and perigee of 10471 km and 272 km, respectively, and an inclination of 75.1°. The attitude of the satellite is stabilized by the spin with the rotation period of about 8 s whose axis is directed to the sun.

The Natural Plasma Wave (NPW) experiment in the PWS system onboard the Akebono satellite is designed to obtain the poynting flux of plasma waves as well as the spectral and polarization measurements over a frequency range from 20 kHz to 5 MHz.

Details of the PWS system have been described by Oya *et al.* (1990). The PY mode operation makes it possible to obtain five components of electric and magnetic field waveforms at eight fixed frequencies. Two sets of crossed dipole antennas with a tip-to-tip length of 60 m detect two components of the electric field. The three-dimensional search coil sensor consists of three square loops with 10 wire turns and an effective area of 0.6 m×0.6 m for picking up three components of the magnetic field. Five components of the wave field signals are fed to the narrow band receivers with 100 Hz bandwidth. The signals are converted into signals with a center frequency of 1 kHz keeping the information of the original amplitudes and phase relations. These 1 kHz signals are transferred to the ground through the telemeter system after converted to a digital form with a sampling frequency of 5 kHz during a sampling period of 10 milliseconds (10 wave trains).

3. Wave Distribution function method

The statistical nature of a waveform data set is obtained by applying Fourier analysis method; namely, a power spectrum of each series data and a cross spectrum between them. For the present data analysis, we use three components of the magnetic field of PY mode data. In this case, the statistic ensemble of a PY mode data set is identified with the spectral matrix,

$$S(\omega)=\begin{pmatrix} \tilde{B}_x^*(\omega)\tilde{B}_x(\omega) & \tilde{B}_x^*(\omega)\tilde{B}_y(\omega) & \tilde{B}_x^*(\omega)\tilde{B}_z(\omega) \\ \tilde{B}_y^*(\omega)\tilde{B}_x(\omega) & \tilde{B}_y^*(\omega)\tilde{B}_y(\omega) & \tilde{B}_y^*(\omega)\tilde{B}_z(\omega) \\ \tilde{B}_z^*(\omega)\tilde{B}_x(\omega) & \tilde{B}_z^*(\omega)\tilde{B}_y(\omega) & \tilde{B}_z^*(\omega)\tilde{B}_z(\omega) \end{pmatrix}, \tag{1}$$

where $\tilde{B}_i(\omega)$ $(i=x, y, z)$ are Fourier components of a magnetic field variation at a frequency ω. Since matrix (1) is Hermitian, there are six independent elements of the matrix, however, these matrix components consist of nine independent values because elements of the matrix can be divided into real and imaginary parts.

In the coordinate system of these measurements the z axis is directed in parallel to an ambient magnetic field vector $\boldsymbol{B}$ and the x-y plane is in perpendicular to $\boldsymbol{B}$ (see Fig. 1). The Wave Distribution Function (WDF), which indicates the distribution of the energy density of electromagnetic waves with respect to a frequency ω and a propagation direction (θ, ϕ), is defined by $F(\omega, \theta, \phi)$ according to the relationship identified by Storey and Lefeuvre (1979, 1980) as follows:

$$S_{ij}(\omega)=\frac{\pi}{2}\sum_m \int_0^{\pi}\int_0^{2\pi} a_{ijm}(\omega, \theta, \phi)\, F_m(\omega, \theta, \phi)\sin\theta\, d\theta\, d\phi, \tag{2}$$

where m denote a mode of electromagnetic wave (X-mode or O-mode electromagnetic waves in the present analysis) and $S_{ij}(\omega)$ is an element of the spectral matrix. The kernel $a_{ij}(\omega, \theta, \phi)$ in the integral eq. (2) is obtained from the dispersion relation of plasma waves as described by Storey and Lefeuvre (1979, 1980). It is then possible to identify the propagation characteristics of electromagnetic waves by solving eq. (2) for $F(\omega, \theta, \phi)$.

In order to obtain $F(\omega, \theta, \phi)$, for a fixed frequency ω, we calculated the discrete

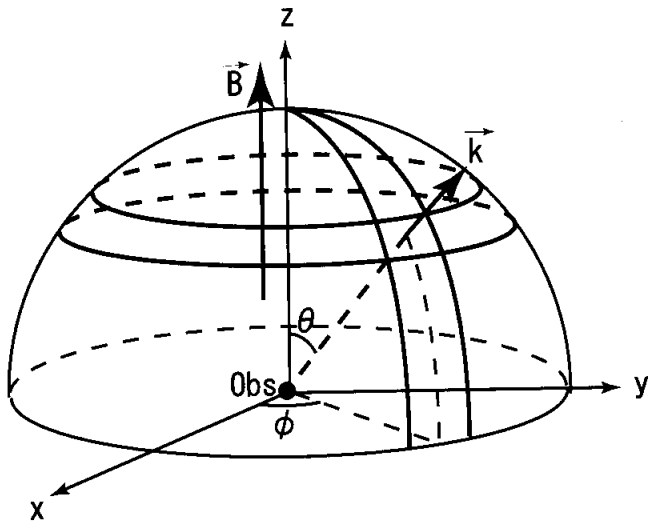

Fig. 1. Coordinate system of the WDF analysis. The z axis is directed in parallel to B (an ambient magnetic field) and the x-y plane is perpendicular to B. The wave normal directions θ and ϕ are colatitude angle and azimuth angle, respectively.

formulation for the θ and ϕ directions for every α (in this present, $\alpha=5^\circ$) around an observation point. Because we are using only magnetic field components of the plasma waves, there is an unavoidable hemispheric ambiguity in the wave normal direction. This ambiguity is resolved by assuming that the observed AKR is propagating in the upward direction. The θ and ϕ directions are divided into $K_\theta=90/\alpha$ and $K_\phi=360/\alpha$ grids. Equation (2) then becomes

$$S_{ij}=\frac{\pi}{2}\sum_{m}\sum_{X,O}\sum_{k}^{K_\theta\cdot K_\phi} a_{ijm}(\omega,\ \theta_k,\ \phi_k)\ F_m(\omega,\ \theta_k,\ \phi_k)\ \sin\theta_k\alpha^2.$$

When we define data vector S consisting of nine independent values of the spectral matrix and discrete WDF vector F_m for each mode, this equation can be rewritten as follows:

$$\begin{aligned} S&=A_X F_X+A_O F_O+e \\ &=(A_X\ A_O)\begin{pmatrix}F_X\\F_O\end{pmatrix}+e, \\ &=AF+e, \end{aligned} \tag{3}$$

where A_m is a $9\times(K_\theta\cdot K_\phi)$ matrix for each mode and an element A_{nkm} is the coefficient of either the real or imaginary part of $(\pi/2)\,a_{ijm}(\omega,\ \theta_k,\ \phi_k)\sin\theta_k\alpha^2$ relating F_{km} to S_n. The 9×1 vector e is the residual errors in the integration. We solved eq. (3) for the unknown vector F by using the approximation of $e=0$.

Based on this method, a solution may be obtained by minimizing the following function E of the mean square of the residual with respect to F:

$$E(\boldsymbol{F}) = (\boldsymbol{AF}-\boldsymbol{S})^t (\boldsymbol{AF}-\boldsymbol{S}). \tag{4}$$

Because the number of given data S is much less than the number of unknown parameters F, this least square problem has a difficulty in the uniqueness. Then, we applied the least square method under the constraint that the solution should be non-negative values for the present problem because $F(\omega, \theta, \phi)$ is defined as the energy density of electromagnetic waves. To minimize $E(F)$ in eq. (4), we used the optimization technique based on the 1D Newton method (see Chiao *et al.*, 1995). This algorithm is implemented as follows:

$$F_i^{n+1} = F_i^n - \frac{\dfrac{\partial}{\partial F_i} E(\boldsymbol{F})\Big|_{F_i = F_i^n}}{\dfrac{\partial^2}{\partial F_i^2} E(\boldsymbol{F})\Big|_{F_i = F_i^n}}, \tag{5}$$

$$F_i^{n+1} = \max\{F_i^{n+1}, 0\}.$$

4. Propagation characteristics of AKR

We applied the WDF method to the PY mode data analysis of AKR emissions observed from 1215 to 1245 UT, 7 February, 1990. In this analysis, we used the data obtained at frequency of 181.5 kHz. Figure 2 shows the dynamic spectra of right-handed (top) and left-handed (bottom) circular polarization components of the AKR emissions during this period. The polarization direction in Fig. 2 is defined with respect to the spin axis of the Akebono satellite. In Fig. 2, the solid line denotes a cyclotron frequency at the spacecraft position. Null data periods in the spectra indicate that the observation was switched from the polarization (PL) mode to the PY mode. During these periods, the solid lines in Fig. 2 indicate the fixed frequencies selected in the PY mode.

Figure 3 shows the intensity ratio of X-mode to O-mode waves. It shows that O-mode waves are dominant within a period from 1215 to 1220 UT that is contrasted with the other period where X-mode waves are dominant. Based on a comparison between Figs. 2 and 3, it is found that the intense AKR emissions at 181.5 kHz in the time period from 1221 to 1245 UT are dominated by X-mode waves and relatively weak AKR emissions are dominated by O-mode waves. This characteristic is consistent with previous AKR observational results (Mellott *et al.*, 1984; Benson, 1985). However, in the present case, O-mode waves also exist with relative power of about 10 percent of X-mode waves even during periods of intense AKR phenomena.

In Fig. 4 the propagation angle between the AKR waves and the geomagnetic filed line is shown for both X-mode (top) and O-mode (bottom) waves at the satellite position. Most of X-mode waves show the propagation angle with smaller than 60° with respect to the local magnetic field line. The important evidence is found within a time period when a lower cut-off frequency of AKR waves is close to a cyclotron frequency at the satellite position, which the propagation direction of X-mode waves tends to be aligned along the geomagnetic field line. O-mode waves appear at two

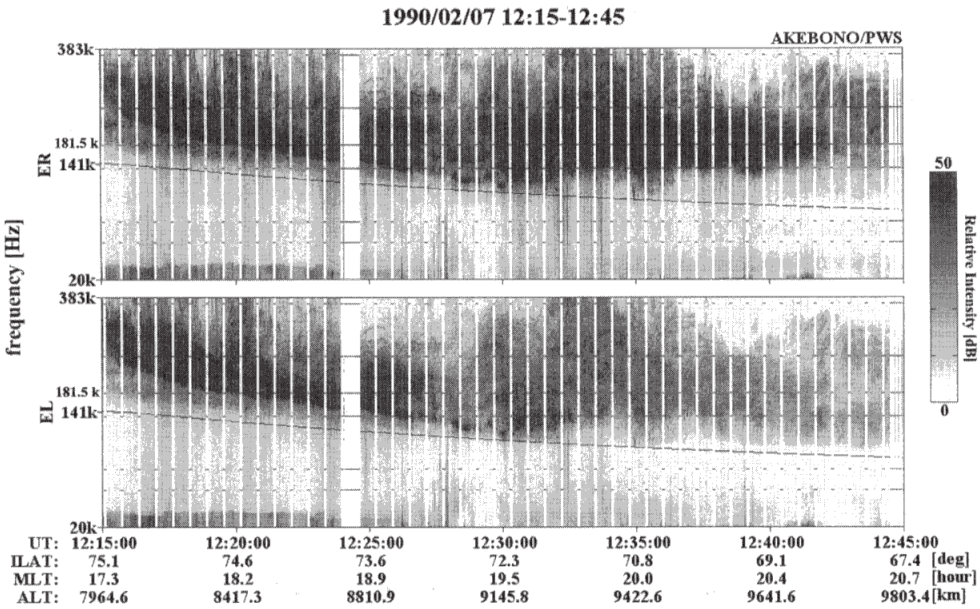

Fig. 2. Dynamic spectra of AKR from 1215 to 1245 UT, 7 February, 1990 showing the right-handed (top) and left-handed (bottom) polarization components with respect to the satellite coordinates. The solid line in the spectra denotes a cyclotron frequency at the spacecraft position. The solid lines during null data periods indicate the fixed frequencies selected in the PY mode.

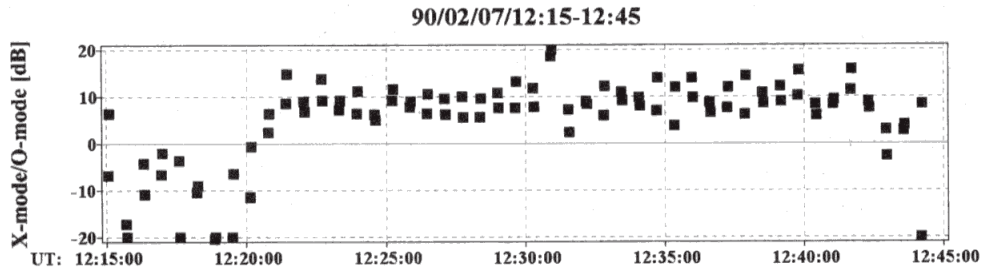

Fig. 3. Time variation of the ratio of the power flux of X-mode to O-mode waves.

groups of propagation angles of 90° and 40°. The O-mode AKR waves propagating perpendicular to the magnetic field are observed in the whole period in the present study. On the other hand, O-mode waves propagating in the vicinity of 40° are observed during the early period of this present case where the O-mode is dominant in the AKR power.

The source location of AKR can be estimated by projecting the propagation direction to a point where the observation frequency coincides with the local cyclotron frequency because AKR emissions are thought to be generated at the cyclotron frequency. In this projection method, effects due to the extent of the solid angle were taken into account because the energy density of the calculated WDF indicates the average energy density on the $5^\circ \times 5^\circ$ mesh for the θ and ϕ directions. In Fig. 5, estimated AKR source locations of X-mode and O-mode waves are plotted as a function

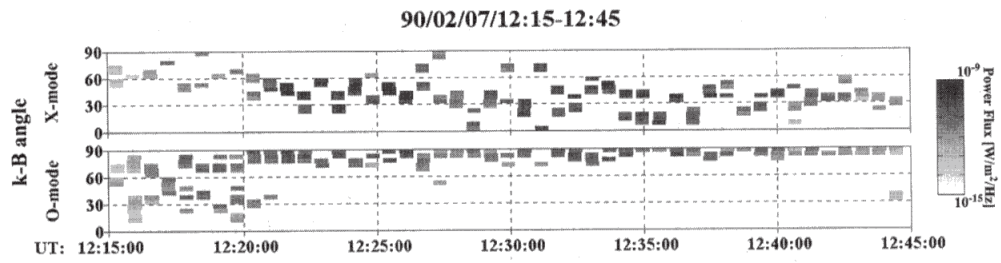

Fig. 4. Time variation of the propagation angle with respect to the local magnetic filed at the satellite position. The power flux of AKR for both X-mode (top) and O-mode (bottom) waves is displayed by using a grayscale code (see a grayscale bar on the right).

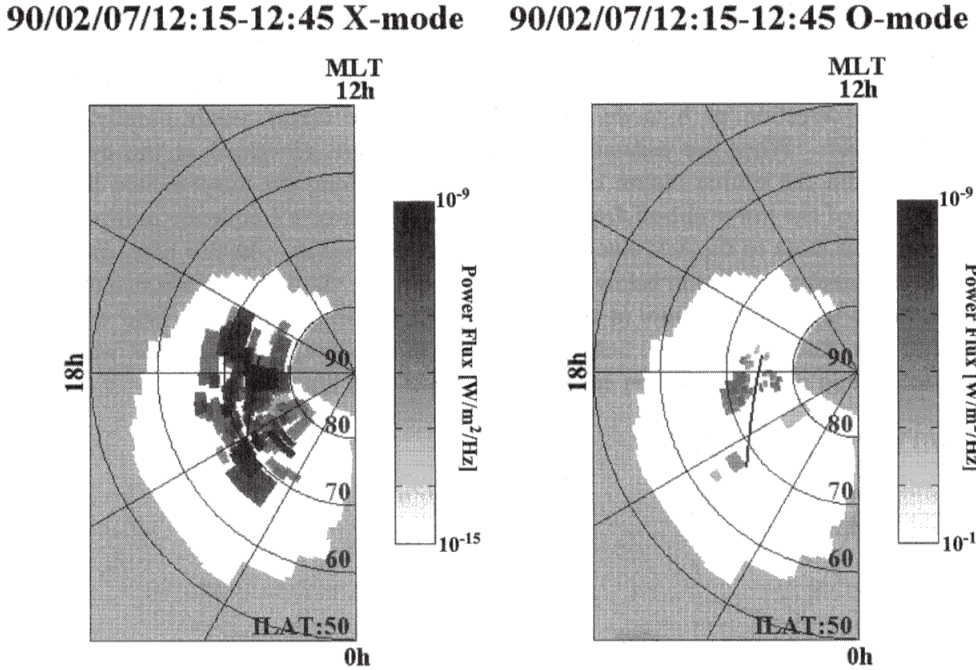

Fig. 5. Distribution of the source locations of AKR estimated from the propagation directions determined using the WDF method as a function of the invariant latitude and the magnetic local time. The power flux of AKR for both X-mode (left) and O-mode (right) waves at the satellite position are indicated by using a grayscale code. The thick solid line denotes footprint of the satellite orbit in the observed period. The white region indicates the field of view of the observation.

of invariant latitude versus magnetic local time. The thick solid line shows the satellite orbit during the observed period. Because we used the data obtained at the observation frequency of 181.5 kHz, the surface of the constant magnetic field intensity with the cyclotron frequency of 181.5 kHz is located below the satellite orbit with the distance of about 1500 km. Then, the source location is limited within a region colored by white in Fig. 5, and the outside region of the field of view is shadowed. Due to the above limit

of the field of view of the observation, the propagation angle of AKR has a limit of less than 70° to the magnetic field line. The power flux for X-mode and O-mode waves at the satellite position is displayed by using grayscale code. Note that Fig. 5 shows only the location data where the propagation line of AKR can intersect with the surface of a constant cyclotron frequency of 181.5 kHz. Due to the same limit of the field of view, the results of perpendicular propagation of O-mode waves cannot be plotted in Fig. 5. On the other hand, the source locations of O-mode waves with the propagation angle of about 40° correspond with those of the intense X-mode AKR waves which is distributed in the evening sector at the invariant latitude range from 65° to 80°.

5. Discussion

5.1. X-mode AKR waves

As it occurred at 1230 UT and 1235 UT in Fig. 4, when the lower cut-off frequencies of AKR are close to cyclotron frequencies at the satellite position, the propagation direction of X-mode AKR waves tends to direct nearly parallel to the magnetic field. When we assume that AKR waves are generated at the cyclotron frequency and the source region of AKR distributes along the auroral field line, the coincidence of the lower cut-off frequency and local cyclotron frequency indicates that the satellite is close to the field line of the AKR source region. In this case, the AKR source locates about 1500 km below the satellite position. So, we conclude that X-mode AKR waves tend to propagate in the direction parallel to the magnetic field when the satellite was close to the source field line. Then, in this case, X-mode AKR waves are radiated within a filled radiation cone of an auroral field line.

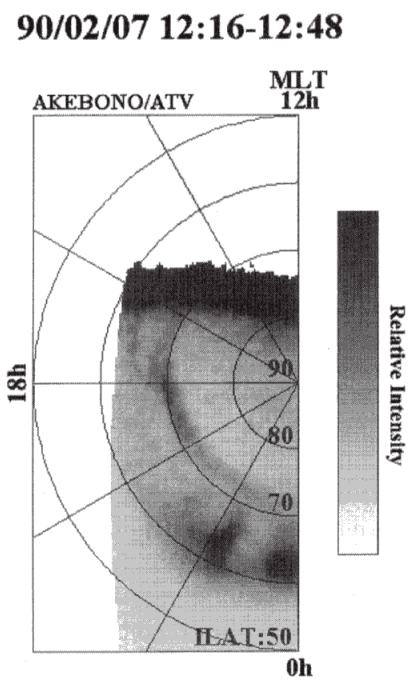

Fig. 6. Polar plots of the auroral image obtained by the ATV system onboard the Akebono satellite. The relative intensity of the aurora is displayed by using a grayscale code.

When we compare the source map shown in Fig. 5 with an image of the Auroral TV camera (ATV) onboard the Akebono satellite in Fig. 6, it is found that the source region of X-mode AKR waves approximately corresponds with the auroral discrete arc. However, differences can be pointed out in detailed signatures which are expected to be caused by the resolution of the WDF method and the scattered propagation nature of AKR waves. The resolution of the WDF method is affected by an error due to the calculation and an error caused by the accuracy of observation data. The calculation error has already been evaluated that it is within a scale of a mesh (5° for the θ and ϕ direction). This influence of the mesh size appeared with the size of a data point plotted in Fig. 5. On the other hand, the data error mainly affects the determination of the ϕ direction that produces the difference of 10° to the authentic direction at the most. This error becomes significant for the distant source from the satellite. The influence of the refraction effect is smaller than the resolution of the WDF method because X-mode AKR waves are mainly refracted in the vicinity of the source. Then differences between the AKR source map and the auroral image can be partly interpreted by the resolution of the WDF method, however, there are still remained differences which cannot be interpreted with this reason. These remained differences between the source mapping and the auroral image are mainly caused by the difference of time resolutions between them. For example, the AKR source found at the point (75° I-Lat, 18 h MLT) was identified by the data obtained at (70° I-Lat, 20 h MLT) 1233 UT. At that time the auroral images were not obtained by the ATV observation.

5.2. *O-mode AKR waves*

The O-mode AKR component with the propagation direction of about 40° is found in the early period of the observation when the O-mode AKR shows dominant power. The power flux of this O-mode AKR was the relatively weak signature that was in a range from $1/10^2$ to $1/10^3$ of the power of the intense X-mode AKR. Because our WDF method can separate between X-mode and O-mode waves only when the weaker propagation mode has a power larger than 0.01 of the other, this O-mode AKR may be masked during the observation period of intense X-mode AKR waves. It is also shown that the source regions of these O-mode AKR waves coincide with those of intense X-mode AKR waves. On the other hand, the O-mode component propagating perpendicular to the magnetic field cannot be interpreted in a same manner. Within assumptions that AKR waves are generated at the cyclotron frequency and the propagation path is a straight line, the source location of these O-mode waves cannot be explained consistently. In this case, O-mode waves are possibly generated as the upper hybrid waves in the dense region as the vicinity of the plasmapause or the edge of the plasma cavity. The azimuthal variation of the propagation direction of these O-mode waves suggests that the source regions are distributed near the auroral oval. Therefore, the O-mode AKR waves with the propagation angle of 90° are possibly generated near the edge of the plasma cavity. The origin of these O-mode waves should be examined in future studies.

6. Summary

Propagation characteristics of the auroral kilometric radiation such as the power flux and propagation direction have been identified for both X-mode and O-mode waves by applying the WDF method to the analysis of the Akebono PY mode data obtained from 1215 to 1245 UT on 7 February, 1990. The results indicated that the power flux of O-mode waves was about 10 percent of the X-mode wave intensity even in strong AKR emissions. We also found that propagation vectors of the X-mode AKR waves tend to fill inside the radiation cone of an auroral field line. On the other hand, O-mode AKR was found to have two different propagation directions, one was at an angle of almost 90° with respect to the local magnetic field and the other showed the angle in the vicinity of 40°. The source locations of AKR for each propagation modes have been estimated from the identified propagation directions. It was shown that the source region of the X-mode AKR coincided with the auroral discrete arc. On the other hand, the source region of the O-mode AKR waves with the propagation angle of about 40° was found to coincide with that of the intense X-mode AKR. The identification of detailed propagation features of AKR waves is due to the WDF method applied by the present study. The overall characteristics as well as fundamental problems concerning the origin of AKR will be resolved based on the extended works applying the WDF method to the observation data obtained by the PWS experiments onboard the Akebono satellite.

Acknowledgments

We would like to thank all the staff of the Akebono satellite team. An auroral image obtained by the ATV system onboard the Akebono satellite were provided by the Akebono Science Data Base (SDB).

The editor thanks Dr. W. Calvert and another referee for their help in evaluating this paper.

References

Benson, R.F. (1975): Source mechanism for terrestrial kilometric radiation. Geophys. Res. Lett., **2**, 52 55.

Benson, R.F. (1985): Auroral Kilometric Radiation: wave modes, harmonics, and source region electron density structures. J. Geophys. Res., **90**, 2753-2784.

Calvert, W. (1985): DE-1 measurements of AKR wave directions. Geophys. Res. Lett., **12**, 381 384.

Chiao, P., Fessler, J.A., Zasadny, K.R. and Wahl, R.L. (1995): Spectral analysis using regularized non-negative least-squares estimation. 1995 IEEE Nuclear Science Symposium and Medical Imaging Conference Record, **3**, 1680 1683.

Gurnett, D.A. (1974): The earth as a radio source: Terrestrial kilometric radiation. J. Geophys. Res., **79**, 4227-4238.

Gurnett, D.A. and Green, J.L. (1978): On the polarization and origin of auroral kilometric radiation. J. Geophys. Res., **83**, 689-696.

Hashimoto, K. (1984): A reconciliation of propagation modes of auroral kilometric radiation. J. Geophys. Res., **89**, 7459 7466.

Kaiser, M.L., Alexander, J.K., Riddle, A.C., Pearce, J.B. and Warwick, J.W. (1978): Direct measurements by Voyagers 1 and 2 of the polarization of terrestrial kilometric radiation. Geophys. Res. Lett., **5**,

857 860.

Means, J.D. (1972): Use of the three-dimensional covariance matrix in analyzing the polarization properties of plane waves. J. Geophys. Res., 77, 5551-5559.

Mellott, M.M., Calvert, W., Huff, R.L., Gurnett, D.A. and Shawhan, S.D. (1984): DE-1 observations of ordinary mode and extraordinary mode auroral kilometric radiation. Geophys. Res. Lett., **11**, 1188-1191.

Morioka, A., Oya, H. and Kobayashi, K. (1990): Polarization and mode identification of auroral kilometric radiation by PWS system onboard the Akebono (EXOS-D) satellite. J. Geomagn. Geoelectr., **42**, 443-458.

Oya, H. (1971): Conversion of electrostatic plasma waves into electromagnetic waves: numerical calculation of the dispersion relation for all wavelengths. Radio Sci., **6**, 1131-1141.

Oya, H. (1974): Origin of Jovian decameter wave emissions-Conversion from the electron cyclotron plasma wave to the ordinary mode electromagnetic wave. Planet. Space Sci., **22**, 687-708.

Oya, H. (1990): Origin of auroral kilometric radiation as conversion of the upper hybrid mode plasma waves. Proc. Jpn. Acad., **66**, 129-134.

Oya, H. and Morioka, A. (1983): Observational evidence of Z and L-O mode waves as the origin of auroral kilometric radiation from the Jikiken (EXOS-B) satellite. J. Geophys. Res., **88**, 6189-6203.

Oya, H., Morioka, A., Kobayashi, K., Iizima, M., Ono, T., Miyaoka, H., Okada, T. and Obara, T. (1990): Plasma wave observation and sounder experiments (PWS) using the Akebono (EXOS-D) satellite - Instrumentation and initial results including discovery of the high altitude equatorial plasma turbulence. J. Geomagn. Geoelectr., **42**, 411-442.

Shawhan, S.D. and Gurnett, D.A. (1982): Polarization measurements of auroral kilometric radiation by Dynamics Explorer-1. Geophys. Res. Lett., **9**, 913-916.

Storey, L.R.O. and Lefeuvre, F. (1979): The analysis of 6-component measurements of a random electromagnetic wave field in a magnetoplasma-I. The direct problem. Geophys. J. R. Astron. Soc., **56**, 255-269.

Storey, L.R.O. and Lefeuvre, F. (1980): The analysis of 6-component measurements of a random electromagnetic wave field in a magnetoplasma-II. The integration kernels. Geophys. J. R. Astron. Soc., **62**, 173-194.

Wu, C.S. and Lee, L.C. (1979): A theory of the terrestrial kilometric radiation. Astrophys. J., **230**, 621 626.

(Received December 7, 2000; Revised manuscript accepted June 6, 2001)